

Scaling properties towards vortex reconnection under Biot-Savart evolution

Y. Kimura¹ and H. K. Moffatt²

¹ Graduate School of Mathematics, Nagoya University,
Furo-cho, Chikusa-ku, Nagoya 464-8604 Japan

E-mail: kimura@math.nagoya-u.ac.jp

² Department of Applied Mathematics and Theoretical Physics,
CMS, Wilberforce Road, Cambridge CB3 0WA UK

E-mail: hkm2@damtp.cam.ac.uk

January, 2017

Abstract. Reconnection of a vortex filament under the Biot-Savart law is investigated numerically using a vortex ring twisted in the form of a figure-of-eight. For the numerical method, the vortex ring is divided into piecewise linear segments, and the Biot-Savart integral is approximated by a summation over the segments with a cut-off method to deal with the singular terms. It is demonstrated that the centre part of the skewed vortex ‘chopsticks’, where the interaction is maximal, tend to approach and accelerate to form a singularity while making a ‘tent-like’ structure as shown by de Waele & Aarts (*Phys. Rev. Lett.* **72** (1994), pp. 482–485). The minimum separation of the chopsticks, the maximum velocity and the maximum axial strain rate show clear scaling exponents near the singularity consistent with Leray scaling for self-similar solutions of the Navier-Stokes equations.

1. Introduction

Vortex reconnection has been studied intensively as a fundamental process both in classical turbulence described by the Navier-Stokes equation and in quantum turbulence as described by the Gross-Pitaevskii equation. As an initial stage of vortex reconnection, nearly anti-parallel segments of vorticity have often been observed experimentally and numerically [1],[2]. Inspired by the recent experiment by Kleckner & Irvine on the dynamics of a trefoil knot vortex [3], we have previously developed a linearised model in which two Burgers-type vortices are driven together by an axisymmetric straining velocity field [4]. With this model, we demonstrated that the time-scale of reconnection is independent of kinematic viscosity ν in the limit $\nu \rightarrow 0$. We also calculated analytically the evolution of helicity during the viscous reconnection process and showed that the initial helicity associated with the two Burgers-type vortices decays to zero during the reconnection process. The possibility of conservation of helicity through

vortex reconnection has aroused great interest for both classical and quantum fluids [5],[6]. The result of non-conservation of helicity contradicts the recent experimental evidence and simulations based on the Gross-Pitaevskii equation. To resolve this contradiction, further study is necessary to clarify the possible difference between classical and quantum reconnections.

In this paper, we extend the linearised reconnection model numerically to include vortex-vortex interaction. We extend the skewed Burgers-type vortices, described as ‘chopsticks’ [7], by adding two ring parts at the ends of vortices to form a closed figure-of-eight vortex (Figure 1), and we calculate the velocity vectors of the segments of the single vortex filament by using the Biot-Savart law. To regularise the singular kernel of the Biot-Savart integral, a cut-off method which simply removes the singular interactions from the integration is employed. With this method, the Biot-Savart integration diverges at a time near the singular time of reconnection. However, scaling properties of the reconnection before the reconnection time t^* can be observed for the minimum separation of the chopsticks, the maximum velocity and the maximum axial straining rate near the singular point, and these scaling properties become clearer as the number of nodes n for the integration is increased.

2. Figure-of-eight vortex

In order to study the nonlinear vortex-vortex interaction during the process of reconnection, we add the two ring parts to the ends of the chopstick vortices to make a single closed vortex-filament curve (Figure 1). As a particular initial condition, we use



Figure 1. Figure-of-eight vortex as a closure of the chopstick vortices.

the following 3D parametrisation of the curve.

$$\begin{cases} x = 0.5 \sin 2\theta \\ y = 2.5 \sin \theta \\ z = 0.05 \cos \theta \end{cases} \quad (0 \leq \theta < 2\pi) \quad (1)$$

A similar ‘Lissajous-elliptic-ring’ initial condition has been previously adopted by Fernandez et al. [8] in a study of the collapse phenomenon using single- and multi-filament Biot-Savart simulations. With this initial condition, we calculate the velocity field using the Biot-Savart law,

$$\mathbf{u}(\mathbf{x}_0) = -\frac{\Gamma}{4\pi} \int \frac{\mathbf{t}(s) \times (\mathbf{x}_0 - \mathbf{x}(s))}{|\mathbf{x}_0 - \mathbf{x}(s)|^3} ds. \quad (2)$$

In this integral, we have assumed that the vortex filament with circulation Γ is thin; $\mathbf{t}(s)$ is the unit tangent vector at arc-length s . The numerical method used is summarised as follows.

- At $t = 0$, we discretise the parameter θ into $\theta_i = 2\pi i/n$ ($i = 0, 1, \dots, n-1$), and calculate the initial condition of each piecewise linear segment accordingly.
- For the corresponding arc-length parameter s_i , the derivative ds_i is defined as

$$ds_i = \begin{cases} (|\mathbf{x}_0 - \mathbf{x}_{n-1}| + |\mathbf{x}_1 - \mathbf{x}_0|) / 2 & (i = 0) \\ (|\mathbf{x}_i - \mathbf{x}_{i-1}| + |\mathbf{x}_{i+1} - \mathbf{x}_i|) / 2 & (i = 1, 2, \dots, n-2) \\ (|\mathbf{x}_{n-1} - \mathbf{x}_{n-2}| + |\mathbf{x}_0 - \mathbf{x}_{n-1}|) / 2 & (i = n-1) \end{cases}$$

- We replace the integral in (2) with a summation over the piecewise linear segments. To deal with the singularity of the integrand, we employ the cut-off method which simply removes the singular pair of segments from the summation. Thus we adopt the following formula for the velocity of the i^{th} segment,

$$\mathbf{u}(\mathbf{x}_i) = -\frac{\Gamma}{4\pi} \sum_{\substack{j=0 \\ j \neq i}}^{n-1} \frac{\mathbf{t}_j \times (\mathbf{x}_i - \mathbf{x}_j)}{|\mathbf{x}_i - \mathbf{x}_j|^3} ds_j \quad (i = 0, 1, \dots, n-1), \quad (3)$$

where $\mathbf{t}_j \equiv d\mathbf{x}_j/ds$ is the tangent vector at \mathbf{x}_j . For the calculation of the tangent vector, discrete FFT is used for spectral accuracy.

- Each segment is advanced according to (3). The 4th-order Runge-Kutta method is used for the time stepping. OpenMP is employed for parallelising the code.

Figure 2 shows the development of the shape of the whole figure-of-eight vortex along the curve of minimum separation $D_{min}(t)$ of the chopstick portions. Four different times ($t = 0, 0.1, 0.2, 0.3$) are chosen, and the projections of the coordinates of the vortex curve on the xy and yz planes are shown. As D_{min} decreases monotonically to 0, the figure-of-eight is deformed mainly at the centre and at the tips. The deformation of the tip parts comes from the self-induction which is approximately proportional to the curvature, while the deformation of the centre part is mostly due to the local interaction of the chopstick portions which leads to a singularity. We see that $D_{min}(t)$ behaves as $\sqrt{t^* - t}$, and this functional form will be used in the next section.

Looking closely at the centre part, we observe that the vortex filaments are slightly twisted and form a nearly anti-parallel vortex pair which translates in the negative x

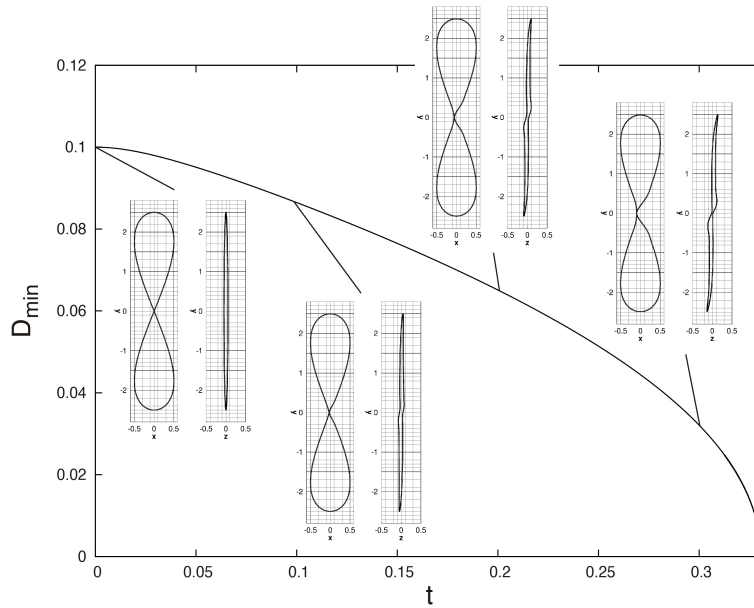


Figure 2. Development of the figure-of-eight vortex along the curve of the minimum distance, $D_{min}(t)$ between the two chopstick portions.

direction with increasing speed. In Figure 3, we magnified the projections of the centre part at four different times before the estimated reconnection time ($t = t^* = 0.330772$, as determined in §3 below).

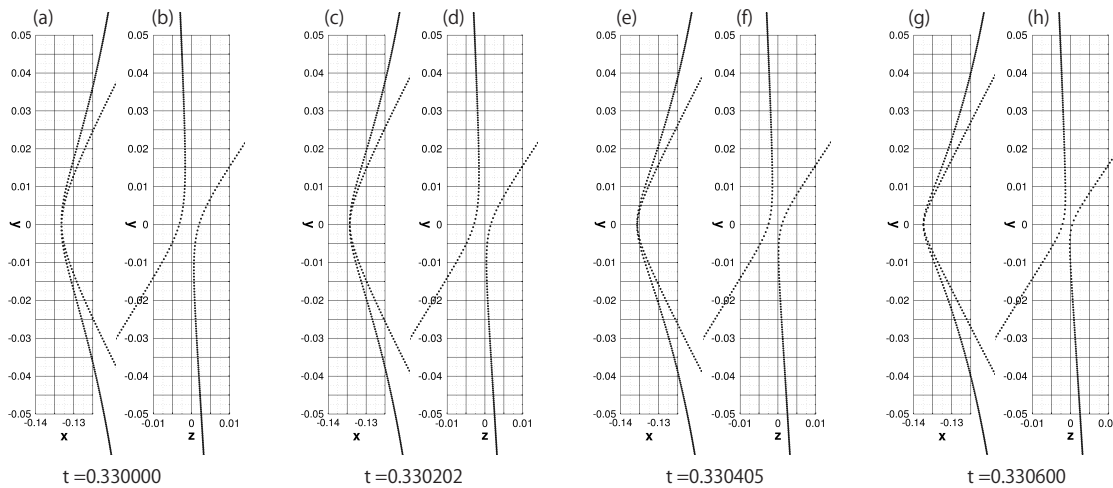


Figure 3. Magnified views of the centre part of the vortex at four different times near the estimated reconnection time, $t = 0.330772$.

In the xy planes near the line $y = 0$, the two curves overlap and produce a hump (Fig3(a), (c), (e), (g)). Production of such a hump is caused by the maximum velocity at the tip due to the strongest interaction between the pair of vortices. From the projections on the yz plane (Fig3(b), (d), (f), (h)), we see that the curves look like a set of hyperbolae which approach the asymptotes as $t \rightarrow t^*$. As the two curves approach the

asymptotes, the interaction at the tips grows rapidly which propels the translation in the negative x direction. This is the essence of the mechanism of producing a singularity during the reconnection of the figure-of-eight vortex.

The mechanism observed for the reconnection of the figure-of-eight vortex agrees with that proposed by de Waele & Aarts [9]. Using numerical simulations of reconnection of two vortex rings, they showed that a tent-like structure is formed by the two colliding anti-parallel vortices before reconnection. This scenario has been confirmed by other researchers using different initial vortex settings.

The present model does not include any regularisation mechanism, and the system blows up as time approaches the singularity. The appearance of a tent-like structure before reconnection implies that some particular vortex geometry may be associated with the singularity. Figure 4, showing velocity vectors on the vortices near the reconnection point at two different times, provides further supporting evidence for this assertion.

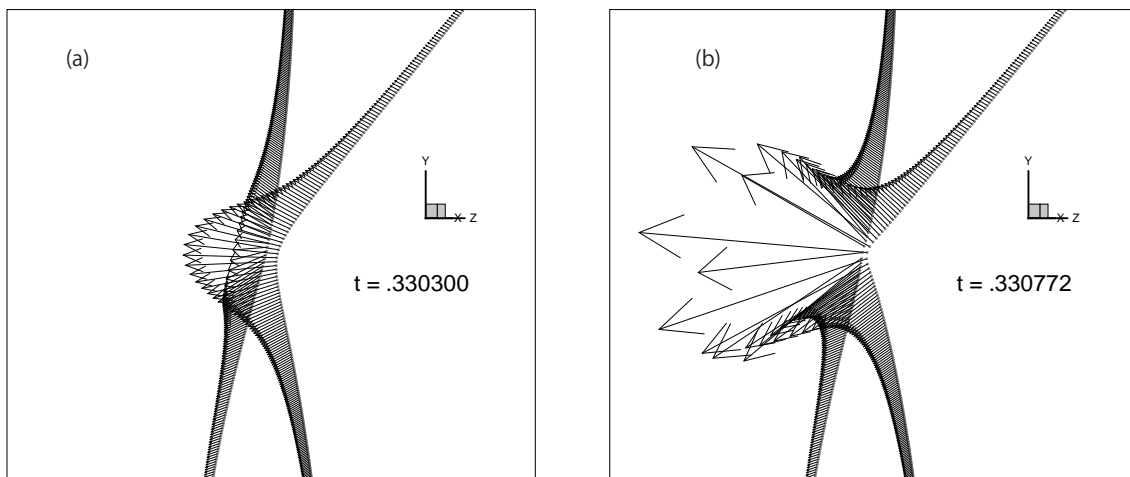


Figure 4. Velocity vectors on the centre part of the vortex at (a) $t = 0.330300$ and (b) $t = 0.330772$.

At $t = 0.330300$, the velocity vectors on the front vortex are continuously and symmetrically changing in magnitude and direction forming a slightly curved smooth surface. The distribution of velocity vectors on the rear vortex is symmetric with the front one, and the surfaces near the tips intersect each other (Fig4(a)). By $t = 0.330772$, the velocity vectors have changed dramatically. In Figure 4(b), we observe that velocity vectors at just a few points in the centre part have quite distinctive magnitude and direction, and that all other velocity vectors tend to form two groups of new anti-parallel vortex segments with continuous distributions. The singular segments appear to be more and more localised, and meanwhile the (presumably) post-reconnection velocity distribution is prepared by other nonsingular segments. It is interesting that even the present regularised Biot-Savart model can anticipate such a post-vortex-reconnection state.

3. Scaling properties towards reconnection

The present model shows clear scaling properties as the reconnection time $t = t^*$ is approached. To determine this time, we plot $(D_{min})^2(t)$ for the case when the number of nodes $n = 2^{15} = 32768$ is the greatest that we used, and extrapolate the straight line to the horizontal axis (Figure 5). From the crossing point, we estimate $t^* = 0.330772$.

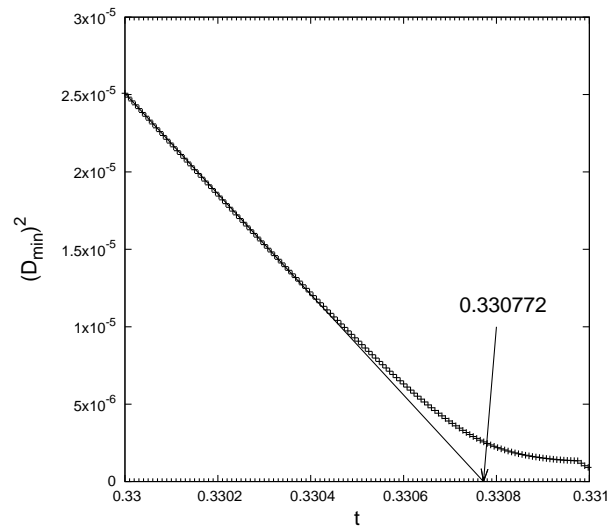


Figure 5. D_{min}^2 , the square of the minimum distance, as a function of time for $n = 2^{15} = 32768$. Extrapolating the straight line, the estimated reconnection time $t = t^* = 0.330772$ is obtained.

Figure 6 shows D_{min} vs. $t^* - t$ on a log-log scale with results for $n = 2^m, m = 11 \sim 15$

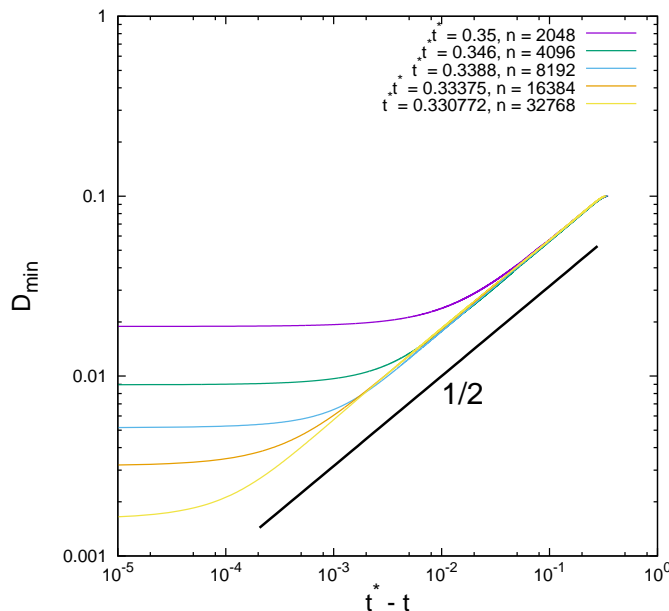


Figure 6. The minimum distance D_{min} vs. $t^* - t$ in the log-log scale.

superposed. After a slight initial adjustment, all curves exhibit the same $1/2$ -power

before levelling off due to the effect of discretisation. As shown in (3) the present numerical model neglects the singular segment from the summation. As the number of nodes n increases, we see that the error decreases in almost inverse proportion with n . We note that the $1/2$ -power for D_{min} has been observed consistently in many studies of both classical and quantum vortex reconnections ([10],[9],[11],[12]). Dimensional analysis suggests that $D_{min} \sim \sqrt{|\Gamma|(t^* - t)}$ which can be verified numerically.

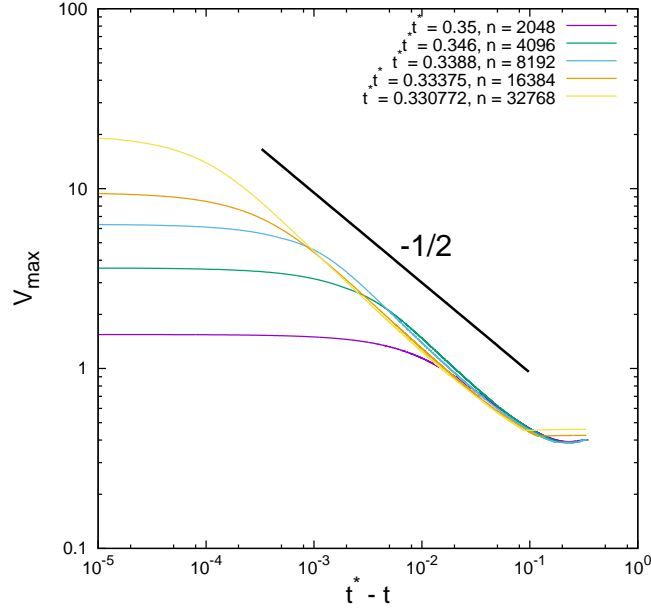


Figure 7. The maximum velocity V_{max} vs. $t^* - t$ in log-log scale.

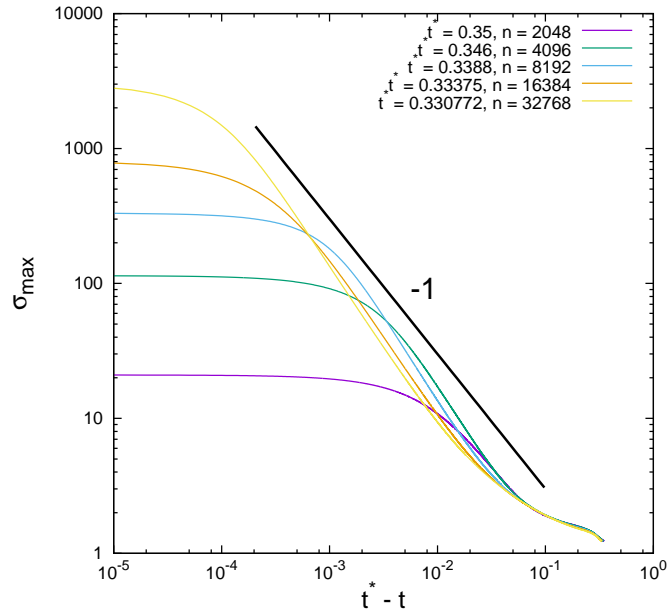


Figure 8. The maximum axial strain rate $\sigma_{max} \equiv \mathbf{t}(s) \cdot d\mathbf{u}(s)/ds$ vs. $t^* - t$ in log-log scale.

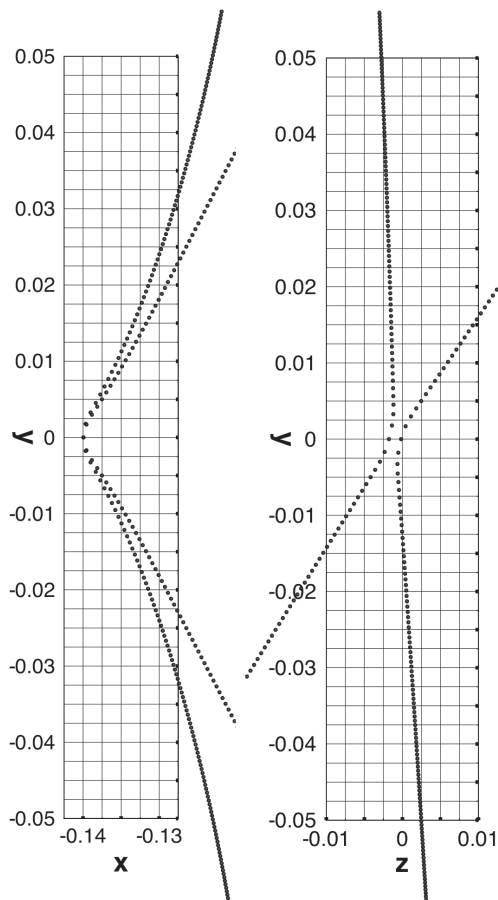


Figure 9. Magnified view of the centre part at the estimated reconnection time $t = 0.330772$. The inflection points are observed on the curve in the xy -projection.

Figures 7 and 8 show the scaling of the maximum velocity V_{max} and the maximum axial strain rate $\sigma_{max} \equiv \mathbf{t}(s) \cdot d\mathbf{u}(s)/ds$ in the log-log scale; these increase as $t \rightarrow t^*$ with approximate scalings $\sim (t^* - t)^{-1/2}$ and $\sim (t^* - t)^{-1}$, respectively.

The above scaling exponents for D_{min} , V_{max} and σ_{max} agree with those proposed by Leray for possible self-similar solutions of the Navier-Stokes equations [14],[15]. For V_{max} and σ_{max} , however, the exponents are slightly larger than the theory and have some dependence on n , indicating some deviation from a self-similar state. Figure 9 provides evidence for this deviation; this shows a blow-up of the centre part at the estimated reconnection time $t = t^* = 0.330772$ for $n = 2^{15} = 32768$. Inflection points on the curves in the xy projection can be observed, suggesting that the centre part has larger velocity than the fringe parts. The excess velocity at the tip may be due to a non uniform distribution of vorticity stretching which deforms the shape of the vortex from self-similarity. The problem of existence of true self-similar solutions for the Biot-Savart model is still an open, and further study is required. (For a recent discussion of the

relation between the approximate self-similar solution and the possible existence of a singularity, see [11], [16]).

Acknowledgments

This work is supported by JSPS KAKENHI Grant Numbers JP24247014, JP16H01175.

References

- [1] Kida, S & Takaoka, M. (1994) Vortex reconnection. *Ann. Rev. Fluid Mech.* **26**, 169–189.
- [2] Laing, C. E., Ricca, R. L. & Sumners, De W. L. (2015) Conservation of writhe helicity under anti-parallel reconnection. *Scientific Reports* **5**: 9224. doi: 10.1038/srep09224.
- [3] Kleckner, D. & Irvine, W. T. M. (2013) Creation and dynamics of knotted vortices. *Nature Physics* **9**, 253258. doi: 10.1038/nphys2560.
- [4] Kimura, Y & Moffatt, H. K. (2014) Reconnection of skewed vortices. *J. Fluid Mech.* **751**, 329–345.
- [5] Scheeler, M. W., Kleckner, D., Proment, D., Kindlman, G. & Irvine, W. T. M. (2014) Helicity conservation in topology-changing reconnections: the flow of linking and coiling across scales. *Pro. Natl. Acad. Sci. USA* **111**, 4647.
- [6] Zuccher, S. & Ricca, R. L. (2015) Helicity conservation under quantum reconnection of vortex rings. *Phys. Rev. E* **92**, 061001(R).
- [7] Kimura, Y. & Koikari, S. (2004) Particle transport by a vortex soliton. *J. Fluid Mech.* **510**, 201–218.
- [8] Fernandez, V. M., Zabusky, N. J. & Gryanik, V. M. (1995) Vortex intensification and collapse of the Lissajous-elliptic ring: single- and multi-filament Biot-Savart simulations and visiometrics. *J. Fluid Mech.* **561**, 329–358.
- [9] de Waele, A. T. A. M. and Aarts, R. G. K. M., "Route to vortex reconnection," *Phys. Rev. Lett.*, **72** (1994), pp. 482–485.
- [10] Siggia, E. D., "Collapse and amplification of a vortex filament," *Physics of Fluids*, **28** (1985), pp. 794–805.
- [11] Hormoz, S. and Brenner, M. P., "Absence of singular stretching of interacting vortex filaments," *J. Fluid Mech.*, **707** (2012), pp. 191–204.
- [12] Zuccher, S., Caliarì, M., Baggaley, A. W. and Barenghi, C. F., "Quantum vortex reconnections," *Physics of Fluids* **24** (2012) 125108 (DOI: 10.1063/1.4772198).
- [13] Paoletti, M. S., Fisher, M. E. and Lathrop, D. P., "Reconnection dynamics for quantized vortices," *Physica D* **239** (2010), pp. 1367–1377.
- [14] Leray, J., "Sur le mouvement d'un liquide visqueux emplissant l'espace," *Acta Math.*, **63** (1934), pp. 193–248.
- [15] Moffatt, H. K., "The interaction of skewed vortex pairs: a model for blow-up of the Navier-Stokes equations," *J. Fluid Mech.*, **409** (2000), pp. 51–68.
- [16] Brenner, M. P., Hormoz, S. & Pumir, A. Potential singularity mechanism for the Euler equations *Phys. Rev. Fluids* **1** (2016), 084503.